Int. J. Heat Mass Transfer. Vol. 17, pp. 275–291. Pergamon Press 1974. Printed in Great Britain

THE TURBULENT BOUNDARY LAYER WITH FOREIGN GAS INJECTION—I. MEASUREMENTS IN ZERO PRESSURE GRADIENT

R. J. BAKER and B. E. LAUNDER

Imperial College of Science and Technology, Department of Mechanical Engineering, Exhibition Road, London, S.W.7., England

(*Received* 30 *November* 1972 *and in revised form* 17 *July* 1973)

Abstract—The results of an experimental investigation are reported of the development of the turbulent boundary layer with surface mass injection. Two injectants were employed, air and freon, with normalized injection rates up to 0·8 per cent of the free-stream mass flux.

For air injection the present data are in very close agreement with the measurements of Simpson *et al.* [3] exhibiting a weaker effect of injection on the local skin friction coefficient than the other investigations of this flow.

With Freon injection, even though density variations occur between the wall and the free stream as high as 4:1, the measured velocity profiles are little different from those obtained with the same rate of air injection. Both mean velocity and concentration profiles become self-preserving after a short initial development region. Comparison of mixing-length and turbulent-Schmidt-number distributions also show no discernible difference from those obtained in uniform density flows.

NOMENCLATURE

c_f, friction coefficient;
c, integration constant in equation (6), (5·75);
J, diffusional flux;
k, mixing length constant;
l, mixing length;
m, mass fraction of foreign gas;
M, mass-transfer parameter, $\rho_w v_w/\rho_G u_G$;
$R_{\delta 2}$, momentum thickness Reynolds number, $\delta_2 u_G/\nu$;
R_x, Reynolds number based upon x;
$R_{\max}$, turbulent Reynolds number $\dfrac{y_G\sqrt{\tau_{\max}/\rho}}{\nu}$;
St_m mass-transfer Stanton number $\dfrac{J_w}{\rho_G u_G(m_w - m_G)}$;
u, streamwise velocity;
u^+, normalized velocity $u/\sqrt{(\tau_w/\rho)}$;
v_w, injection velocity at wall;
x, distance in streamwise direction;
x_0, virtual origin;
y, normal distance from surface;
y^+, normalised cross stream distance $\dfrac{y(\sqrt{\tau_w/\rho})}{\nu}$;
y_F, thickness of concentration boundary layer;
δ_1, displacement thickness;
δ_2, momentum thickness;
ν, kinematic viscosity;
σ, Schmidt/Prandlt number;
τ, shear stress;
Φ, normalized mass fraction $\dfrac{(m_w - m)}{(m_w - m_G)}$;
ψ^+, function defined in equation (5);
ρ, density.

Subscripts

G, free stream value;
m, refers to mass-transfer parameters;
0, value in absence of transpiration;
t, equivalent turbulent value;
w, wall value.

1 INTRODUCTION

INTEREST in the behaviour of the turbulent boundary layer on a porous surface was stimulated principally by developments within the gas-turbine industry over the last decade. By the early 1960's it had become clear that, to attain the projected increases in turbine inlet temperature from one generation of engine to the next, a more effective means of protecting blade surfaces would soon be needed than that offered by conventional internal blade-cooling techniques. The passage of air *through* the blade surfaces provided just such a means of achieving the necessary thermal protection. Two main cooling processes have been considered: "film cooling" where, in an idealized model, cool fluid is injected through a slot in the blade surface as nearly tangential with the surface as design considerations permit; and "transpiration cooling" wherein the blade material is porous and the passage of cooling fluid from the interior to the exterior of the blade takes place over all, or nearly all, of the blade surface.

Recently prospects seem to have receded of actually employing in commercial use a pure version of a transpiration-cooled blade. Nevertheless, the boundary layer developed on a permeable wall remains of considerable interest because surface mass transfer will radically alter the distribution of shear stress across the flow from that found on an impermeable wall. Experimental data of such flows can thus offer a searching test of the appropriateness of any model proposed for simulating the turbulent flux processes.

The earlier investigations of the problem (e.g. [1, 2]) served mainly to show what considerable care in the design of the test section was needed to secure a two-dimensional, well identified transpired boundary layer. More recently the work of Simpson [3] set new standards in respect of the scope of the investigation and of the precautions taken to secure accuracy; the data obtained in this study suggested a weaker influence of blowing on surface friction than earlier investigations. Squire [4] concluded from a re-examination of the data, however, that the quoted variation of c_f was not that which was implied by a 2-dimensional momentum balance.

The present experimental study has provided extensive new data of transpired boundary layers both for air and for freon injection. From the former data we attempt to resolve the discrepancies between [3] and [4]. The measurements of freon injection extend data of heavy-gas transpiration to density ratios and injection rates an order of magnitude higher than those measured by Dunbar and Squire [5]. Extensive measurements have also been made of flows in non-zero pressure gradients; these data are presented in a companion paper [6] which considers principally the problem of predicting the behaviour of transpired boundary layers.

Although the present paper is concerned mainly with experiments, it will serve later discussion to summarize the outcome of applying the Prandtl mixing-length hypothesis to flow near a permeable wall. Provided pressure gradients are small or absent, streamwise convective transport of momentum is negligible over the 15 per cent of the boundary layer closest to the wall. For this region, the momentum and continuity equation may be combined to yield:

$$\rho v_w u = \tau - \tau_w. \tag{1}$$

Except in the immediate vicinity of the wall, molecular contributions to the shear stress are negligible; the total stress may thus be replaced by the turbulent stress, τ_t which by the mixing-length hypothesis may be replaced by:

$$\tau_t = \rho l^2 \left|\frac{\partial u}{\partial y}\right| \frac{\partial u}{\partial y} \tag{2}$$

where l is the so-called mixing length. Near an impermeable wall the linear mixing-length variation:

$$l = ky \tag{3}$$

is known to agree with experiments. Assuming, therefore, that blowing does not affect the mixing length profile, equations (1)–(3) may be combined to give:

$$\frac{\mathrm{d}y^+}{ky^+} = \frac{\mathrm{d}u^+}{(1 + v_w^+ u^+)^{\frac{1}{2}}} \tag{4}$$

where plus superscripts denote that the quantities have been non-dimensionalized with the friction velocity, $\sqrt{(\tau_w/\rho)}$ and kinematic viscosity. Integration of (4) followed by obvious manipulation gives the following expression for the variation of velocity with distance from the wall:

$$\psi^+ \equiv 2u^+/[(1 + v_w^+ u^+)^{\frac{1}{2}} + 1] = \frac{1}{k} \ln y^+ + f\{v_w^+\} + c. \tag{5}$$

The form of (5) is chosen so that the function of integration, $f\{v_w^+\}$ is zero for no transpiration; the velocity profile then takes the familiar form:

$$u^+ = \frac{1}{k} \ln y^+ + c \tag{6}$$

where the constants k and c are equal to about 0·42 and 5·5 respectively.

The appropriate functional form of $f\{v_w^+\}$ was, and still is to some extent, a fundamental point of

controversy. Its value depends on the distribution of l in the immediate vicinity of a wall where equation (3) is not valid even on an impermeable wall. Here we mention that Stevenson [7] deduced from his own and McQuaid's [8] data that $f(v_w^+)$ was effectively zero while Black and Sarnecki [9] proposed that:

$$f(v_w^+) = \frac{2}{v_w^+}[(1 + v_w^+ u_a^+)^{\frac{1}{2}} - 1] + \frac{1}{k}\ln\left[\frac{v_w^+}{\ln(1 + v_w^+ u_a^+)}\right] + c \qquad (7)$$

a form which corresponded closely with an earlier proposal of Rubesin [10] and which displays somewhat greater sensitivity to v_w^+ than Van Driest's [11] recommendation.

The data of Simpson *et al.* [3] agreed with none of the above proposals, displaying about twice the dependence on v_w^+ implied by equation (7). In section 3 we draw comparison among the various proposals for $f(v_w^+)$ and the present data. First, however a short description of the apparatus and validation tests are provided.

2. APPARATUS INSTRUMENTATION AND PRELIMINARY TESTS

Measurements were made in the open circuit test facility shown schematically in Fig. 1. The primary air flow was provided by a centrifugal fan driven by a 10 h.p. A.C. synchronous motor; it was supplied to the test section by way of a settling chamber and a 12 to 1 contracting section producing a turbulence level at the exit of less than 0·25 per cent in a stream at nominally 100 ft/s. The test section was 48 in long with a 12 in × 8 in cross section, and utilized an adjustable roof to provide streamwise pressure gradients.

The test plate which formed the floor of the test section included a boundary layer bleed, and porous and impermeable sections which could be assembled in different arrangements. The porous surface was provided by a porosint sintered bronze plate 20 in × 12 in × 0·25 in made from grade A particles. In general the pressure drop through the plate was sufficiently large to ensure that streamwise pressure gradients along the plate had a negligible effect upon local injection rate; in cases where the injection rate was low and the streamwise pressure gradient high, a correction to the local injection rate was calculated from the local pressure drop.

The secondary gas flow, supplied either from a bank of bottles or from a compressed-air line, entered at the base of the plenum, as shown in Fig. 2. The secondary flow rate was metered by a specially calibrated set of interchangeable orifice plates, and except for the highest injection rate with bottled gas, was held steady within 1 per cent over the duration of any test.

Total head profiles across the boundary layer were obtained by means of a conventional pitot tube with an internal tip height of 0·005 in. Static pressure profiles were measured using a standard four-hole probe of the same geometrical proportions as the total head probe (in an attempt to eliminate any blockage effects caused by the probes). Concentration measurements employed a probe identical to the total head probe except that small bore tubing was used internally to reduce flushing times of gas samples. All the probes fitted into a boundary layer traversing mechanism with a 2-in micrometer adjustment and electrical sensing device for zeroing the probes.

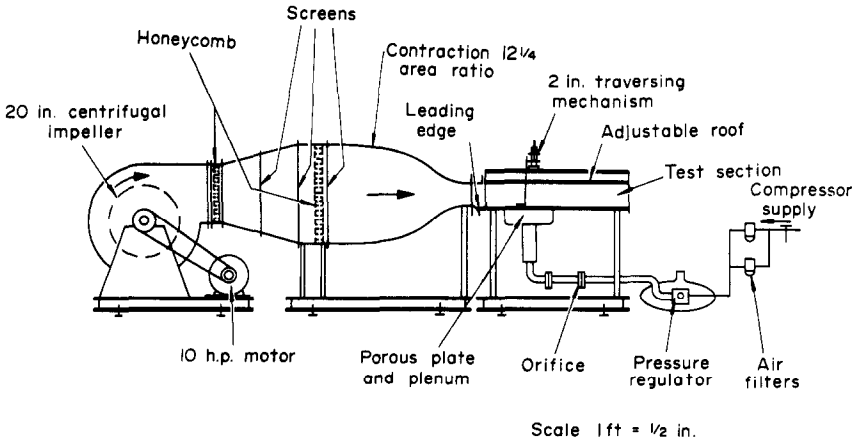

FIG. 1. General wind tunnel arrangement.

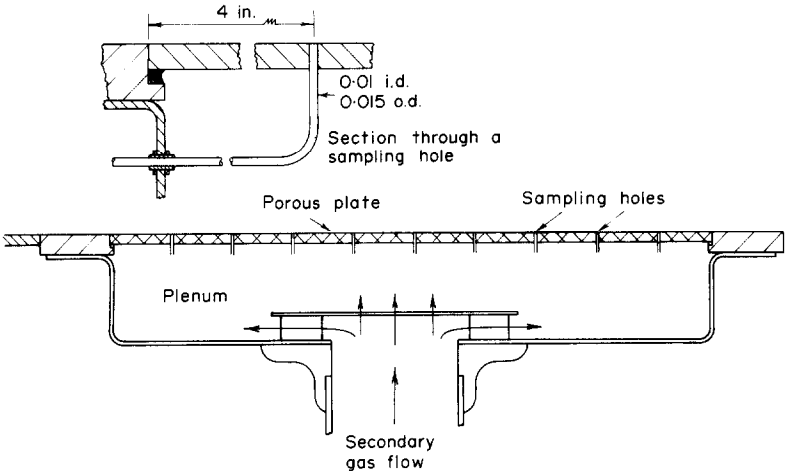

FIG. 2. Porous plate.

The total and static pressures obtained with the *probes*, were measured with a specially constructed vertical U-tube reservoir-type manometer in which a telemicroscope was employed to detect changes in height of the liquid column. This instrument was more reliable and had a faster response than an inclined manometer while retaining a sensitivity of 0·001 in of water.

Concentration measurements were made with a Pye '104' Isothermal Katharometer Chromatograph which had been extensively modified to produce a continuous sampling instrument. The modification enabled readings to be taken more quickly but had the effect of reducing sensitivity of the instrument compared with its original mode of operation. Since, however, we were interested in measuring relatively high gas concentrations the loss of sensitivity was tolerable. Basically, equal flow rates of the sample and a reference air stream, were drawn through the Katharometer head located in a constant temperature* oven. The different thermal conductivities of the two streams was manifested by a voltage imbalance recorded by the Katharometer, the calibration of which had previously been determined by passing known mixtures through the instrument. This calibration was generally insensitive to 5 per cent imbalances in the flow rates of the two streams. Figure 3 shows that the concentration was invariant over a sampling rate range of 10–100 ml/min; a standard sampling rate was therefore adopted of 60 ml/min which corresponded to a probe tip velocity of approximately 10 ft/s.

* Within 0·1°C at 50°C.

The measurement of the *surface* concentration level was achieved by a technique which involved withdrawing samples through tubes (0·015 in o.d.) imbedded in the plate with their openings flush with the surface, as shown in Fig. 2. On testing the instrumented plate, it was discovered that the surface concentration still increased as the sampling rate was lowered to 10 ml/min. As this was the lowest sampling rate that could be tolerated through the Katharometer, we resorted to a multi-hole sampling technique in which samples were drawn from all eight holes on the plate at once: the reading was then repeated except that the tube at the point where the concentration was required was disconnected. The concentration at the point was then obtained from the formula

$$m_w = 8m_{w,8} - 7m_{w,7} \tag{8}$$

where $m_{w,8}$ and $m_{w,7}$ denote the average wall-concentration levels obtained with 8 and 7 tubes respectively. Figure 3 shows that with this technique, the indicated wall concentration was constant in value when the flow rate through any *single* hole was below 3 ml/min, i.e. 0·25 ft/s.

The variation of porosity over the plate surface was measured and found to be uniform to within ± 5 per cent along the centre line. There was, in fact, a small variation in porosity from front to rear which is well fitted by the equation:

$$v_{\text{local}} = \bar{v}(1{\cdot}0 - 0{\cdot}0248x + 0{\cdot}00342x^2 - 0{\cdot}000101x^3) \tag{9}$$

where x denotes the downstream distance in inches from the start of the porous section. The porosity

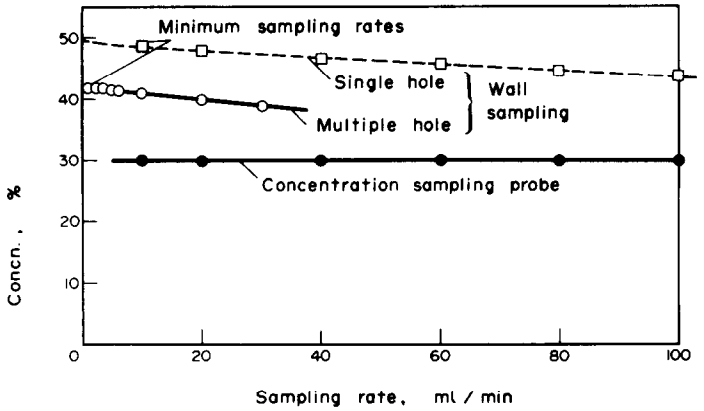

FIG. 3. The effect of sampling rates on wall and probe concentration measurements.

distribution was measured again half way through the test programme; no significant differences were observed.

The two-dimensionality of the flow through the test section was explored with the *impermeable* test plate inserted. Mean velocity profiles were measured at 2-in intervals along the plate and the local skin friction coefficient, c_f, derived from a mean momentum balance as described in the Appendix 1. The velocity profiles were plotted in "universal" coordinates, $u^+ \sim y^+$, as shown in Fig. 4; it is evident that for an appreciable region near the wall the velocity profiles at all positions collapse onto a single curve, and that a straight line fitted to this region has the form:

$$u^+ = \frac{1}{0{\cdot}425} \ln y^+ + 5{\cdot}75. \qquad (10)$$

Equation (10) implies, over the region of interest, a relationship between u^+ and y^+ almost identical with those proposed by Patel [12] and many other workers. We may thus reasonably infer that the values of wall

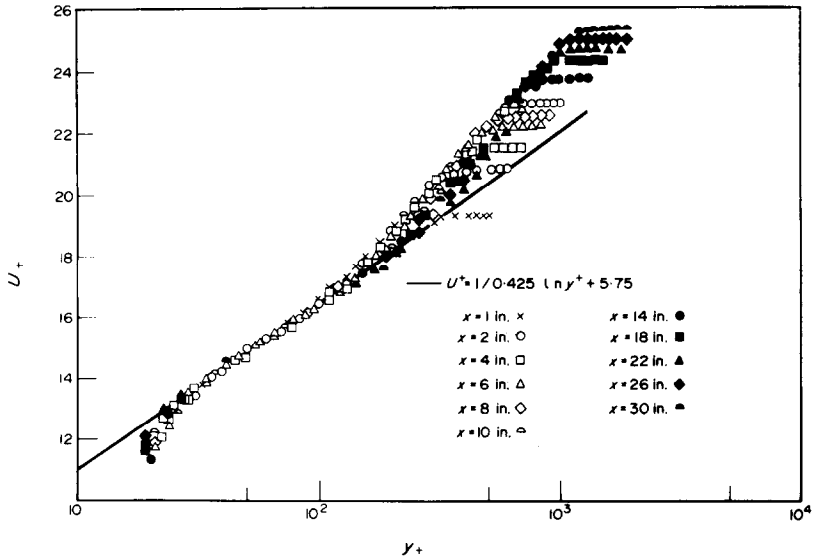

FIG. 4. $U_+ - y_+$ profiles along the impermeable surface in zero pressure gradient.

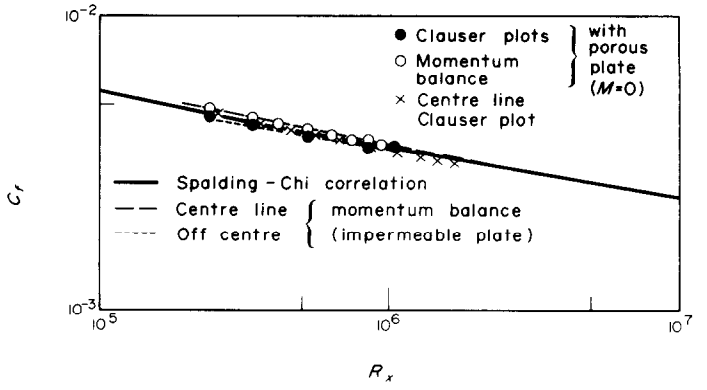

FIG. 5. Skin-friction coefficient vs Reynolds number R_x—comparison of various measurements on the impermeable and porous surface.

shear stress deduced from a 2-dimensional momentum balance are substantially correct and, hence, conclude that the flow is indeed sensibly two dimensional.

The final preliminary test was to ascertain that the porous plate was aerodynamically smooth. Figure 5 compares the variation of c_f along the smooth and impermeable plates. The differences amount to no more than 4 per cent and may therefore be thought negligible. Moreover, both sets of data are in excellent agreement with the Spalding–Chi [13] correlation for flat-plate boundary layers.

3 PRESENTATION AND DISCUSSION OF EXPERIMENTS

Figure 6 shows mean velocity profiles for four levels of air injection rate; y_G denotes the height above the wall where the velocity is 99 per cent of that in the free stream. There are two main features of these flows: firstly, the velocity gradient (outside of the viscous sublayer) increases as the level of M increases; second, for any given M the profiles for $x > 10$ in display close similarity.

Among the most difficult to measure—yet most interesting—properties of a transpired boundary layer is the wall shear stress. The difficulty of measurement arises because the skin friction coefficient is usually found as the small difference between two large terms in the integral momentum equation. In the present study c_f was determined by a least-squares fit to the measured momentum thickness, some details of which are given in Appendix 2. Typically, the standard deviation of the fit was less than 0·2 per cent of δ_2 at a mid plate position, compared with 0·6 per cent obtained by reprocessing Simpson's [3] data and 2 per cent using Simpson's original method. Our fitting procedure is superior to Simpson's though this does not mean that the present data are necessarily the more accurate.

The calculated variation of c_f along the plate is shown in Fig. 7; numbers in parentheses denote the estimated percentage uncertainty in the values quoted. The curves become steeper at high Reynolds numbers because the mass transfer rate increases somewhat

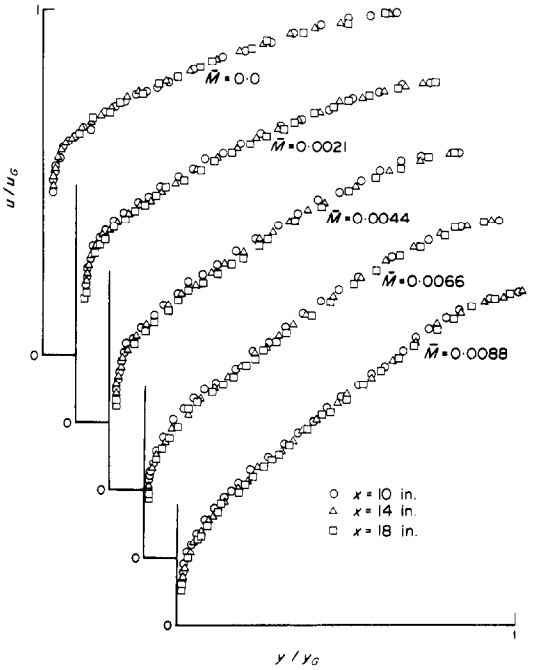

FIG. 6. Air injection velocity profiles.

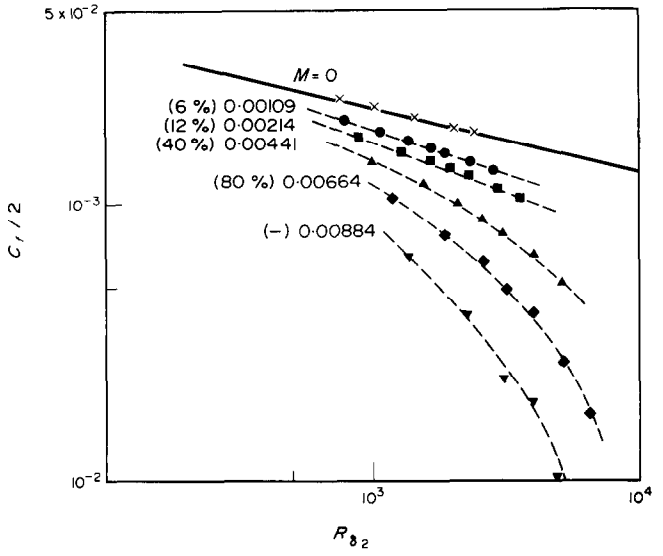

FIG. 7. Skin friction coefficient vs Reynolds number $R\delta_2$ for zero pressure gradient with air injection.

towards the downstream end of the plate. Figure 8 shows, for $R_x \approx 10^6$, the variation of c_f/c_{f0} with blowing parameter, $2M/c_{f0}$; c_{f0} denotes the level of skin friction at the same R_x on an impermeable wall. It is seen that the present data are in very close agreement with those of [3]. There the matter might rest

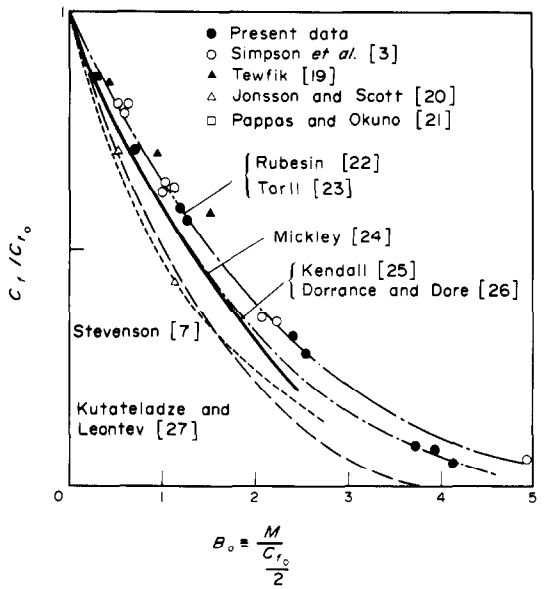

FIG. 8. Comparison of skin friction data for different blowing rates.

were it not that Squire [4] reprocessed the data of Simpson *et al.* and concluded that the quoted skin friction coefficients were obtained from a poor fit to the measured $\delta_2(x)$ variation. The values deduced by Squire showed, the resultant c_f varying little along the plate. We have also reanalysed the Simpson data using the present numerical procedure; the outcome is shown in Fig. 9. Evidently, the present reprocessing tends to support the values deduced by Squire, though for $R_x = 10^6$ (which was the value of length Reynolds number for the data shown in Fig. 8) the reprocessed values agree closely with those of the original data.

With the skin friction determined, we may now examine the validity of equation (5) for the variation of velocity with y^+. From Fig. 10 it is seen that for $y^+ < 150$ there is a region of the profile where the $\psi^+ \sim y^+$ profile is linear with the same slope as occurs on an impermeable surface. Increasing the level of blowing displaces the profile downwards on these axes and leads to the logarithmic region of the profile extending to smaller values of ψ^+.

The function $f(v_w^+)$ which appeared in equation (5) has been evaluated from our data and plotted in Fig. 11 along with a number of proposals for the function implied by earlier studies. Two lines are shown for the Simpson data, one being that proposed by Simpson, the second being that which we deduced from re-examining the original data. The present results lie between the Simpson (reprocessed) and Black and Sarnecki curves though closer to the former.

The influence of $f(v_w^+)$ may be eliminated from the

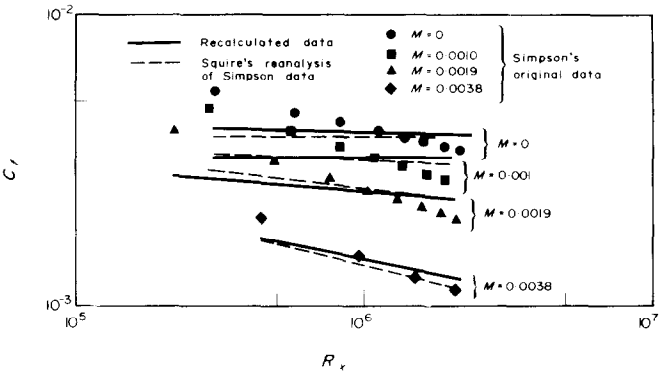

FIG. 9. Re-analysis of Simpson's skin-friction data.

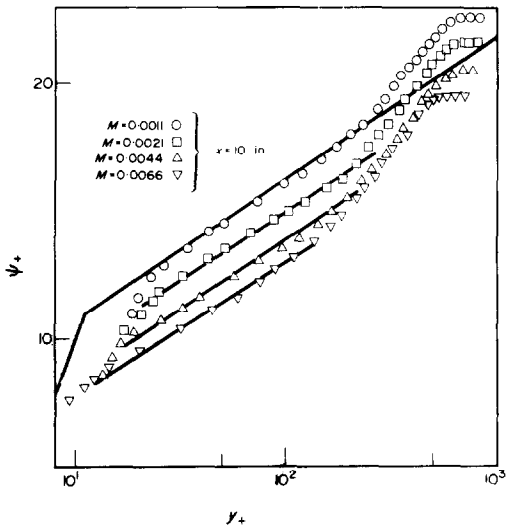

FIG. 10. $\psi_+ - y_+$ velocity profiles for zero pressure gradient with air injection.

transpired velocity curves by plotting them in defect co-ordinates, Figs. 12 and 13; for no blowing, this presentation is identical with the standard velocity-defect plot. All the data except the profile at $x = 4$ in collapse very nearly onto a single curve. Coles [14] has proposed that for a normal unblown boundary layer, the maximum departure of the defect profile from the semi-logarithmic law should be about 2·7 (the data which Coles accepted as "normal" showed variations about this value as large as ± 15 per cent). Except for the profile at $x = 4$ in, the present data display a maximum departure from the logarithmic line within these limits. We thus conclude that in terms of the transpired defect velocity, $(\psi^+ - \psi_G^+)$, the velocity profile for developed blown boundary layers is essentially the same as that of the unblown profile except for the viscosity-dependent zone immediately adjacent to the wall. The word "developed" was inserted above to indicate that, when transpiration does not begin at the leading edge, we must exclude from consideration an initial transpired region. This

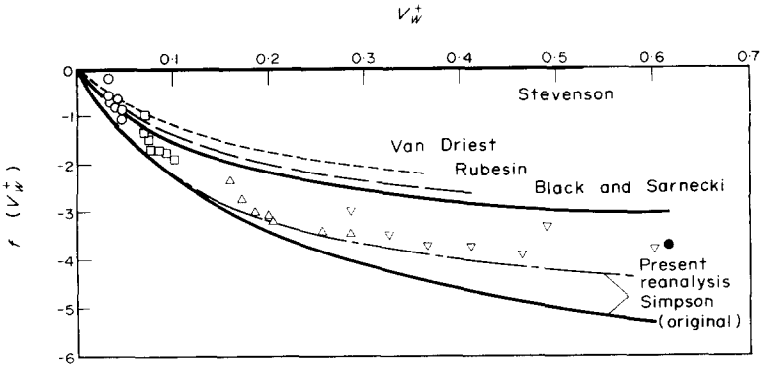

FIG. 11. The variation of $f(V_w^+)$ with injection.

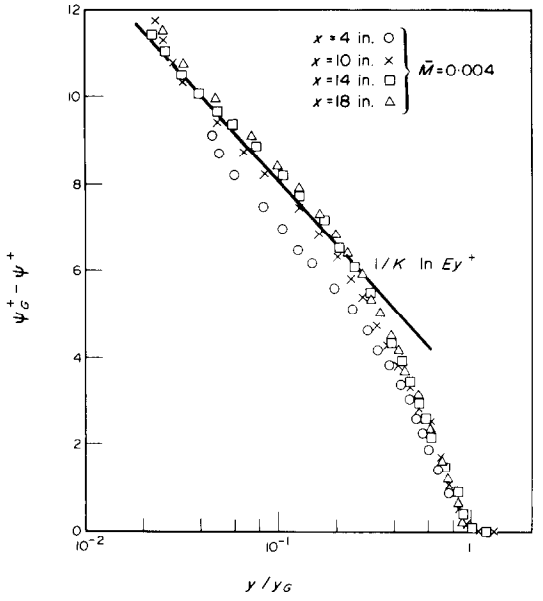

FIG. 12. Air injection velocity defect profiles.

is because the effects of blowing at the surface will require some distance to work through to the outer edge of the boundary layer. We believe this is why the profile at $x = 4$ in appears anomolous.

To obtain the mixing length distribution across the flow, the shear stress was first determined by the method outlined in Appendix 1. Then, by differentiating the mean velocity profile, l was calculated from equation (3). The results of the processing are shown in Fig. 14 for sixteen profiles spanning all the blowing rates. The l-profile can be quite reasonably described by a ramp distribution similar to that proposed by Escudier [15]: over the inner 15 per cent of the flow the data collapse, with little scatter about the line $l = 0{\cdot}425y$, and over the outer 80 per cent of the shear flow the level of mixing length for any profile is practically constant. There is, however, a fair amount of ordered variation in the height of the plateau over this outer region. The mixing length decreases both with increasing distance downstream and with increasing blowing levels. We re-examine this behaviour later in conjunction with the comparable data for freon injection.

The final comparison for air injection is derived from measurements of wall concentration when a tracer of helium (about 2 per cent by volume) was introduced into the secondary air supply to show the effect of transpiration on the Stanton number. (See Baker [16] for details of modifications in sampling procedure from that described in section 2 for freon injection.) In our experiments, St_m was found from measurements of the mass fraction of helium in the settling chamber, m_c and at the external plate surface, m_w together with the normalised injection rate M; it is readily deduced that:

$$St_m = M(m_c - m_w)/m_w. \tag{11}$$

Equation (11) could not of course be used to determine St_{m0}, the Stanton number in the absence of injection. Instead, from a knowledge of c_{f0}, St_0 at the same position was determined from:

$$St_0 = \frac{c_{f0}}{2}(\sigma)^{-\frac{2}{3}}. \tag{12}$$

For small concentrations of helium $\sigma^{-\frac{2}{3}}$ is approximately 2·6. It is seen from Fig. 15 that the present mass-transfer-based Stanton-number ratio is in almost

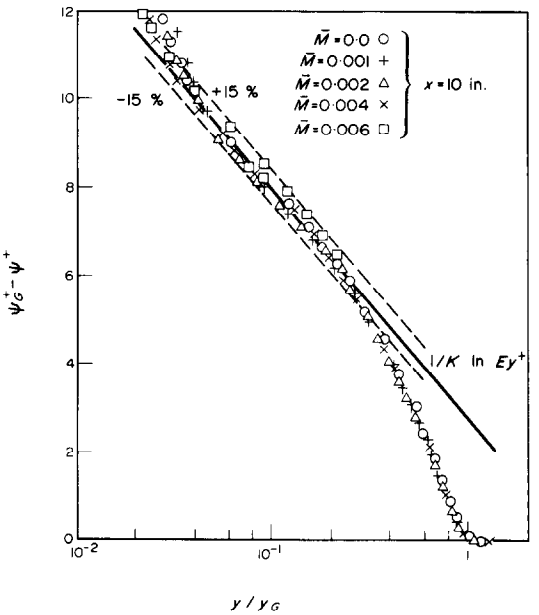

FIG. 13. Air injection velocity-defect profiles.

perfect agreement with the best line through the heat-transfer data of Moffat and Kays [17]. The result suggests that the technique of withdrawing a sample through the wall provides a reliable means of determining the wall concentration values.

We now turn to the data for freon injection. First it is seen from Figs. 16 and 17 that the velocity and concentration profiles on linear scales are very nearly self preserving over the downstream half of the plate. Indeed the ϕ and u/u_G profiles for any level of blowing

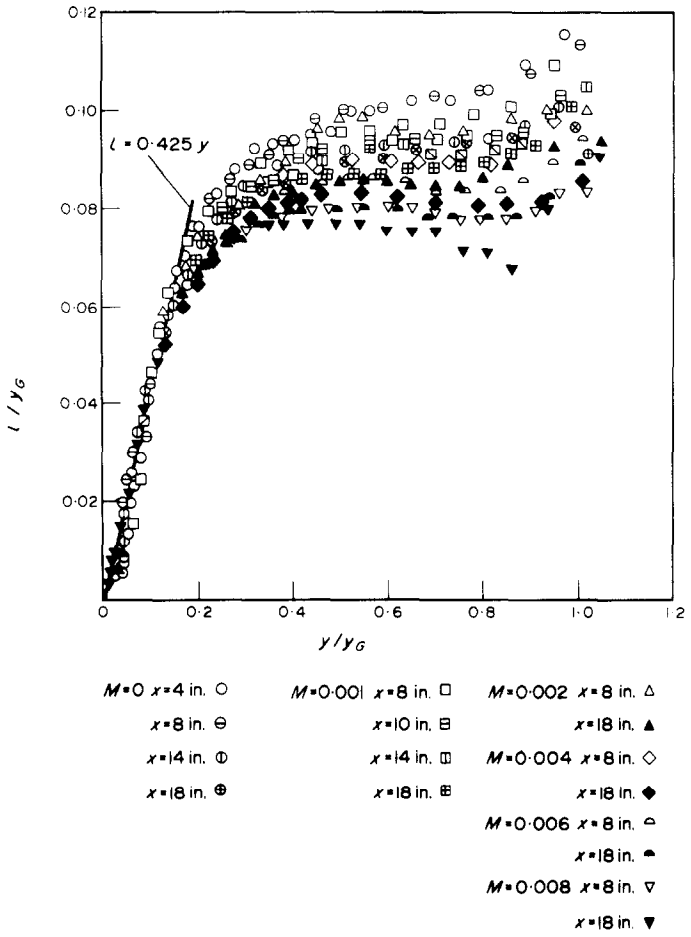

FIG. 14. Mixing length distributions for various air injection rates in zero pressure gradient.

rate are very nearly the same, indicating that over most of the flow the effective Prandtl/Schmidt number is close to unity (a matter to be confirmed directly below). As M is successively raised, the profiles are progressively pushed down near the wall. Figure 18 shows there is no significant difference between the velocity profiles for air or freon injection at the same injection rate in the fully turbulent part of the layer; because of the very high density fluid injected near the wall, however, the profile of ρ_u for $M = 0{\cdot}0078$ displays a peak. Figure 19 shows velocity profiles for freon injection in transpired velocity defect coordinates. Over the outer 95 per cent of the boundary layer the profiles for the four injection rates collapse with very little scatter onto a single curve which, however, is not coincident with that for an impermeable surface. The result indicates that at *lower* injection rates than examined here the profile

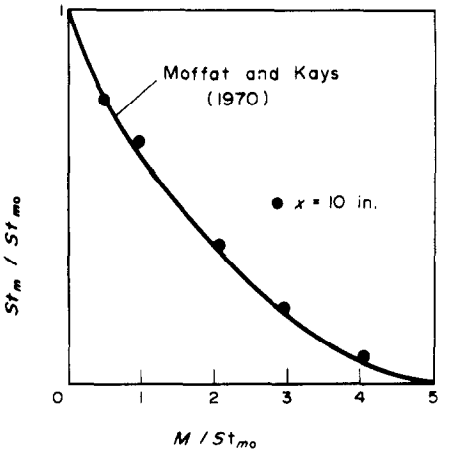

FIG. 15. Comparison of helium tracer and heat transfer data.

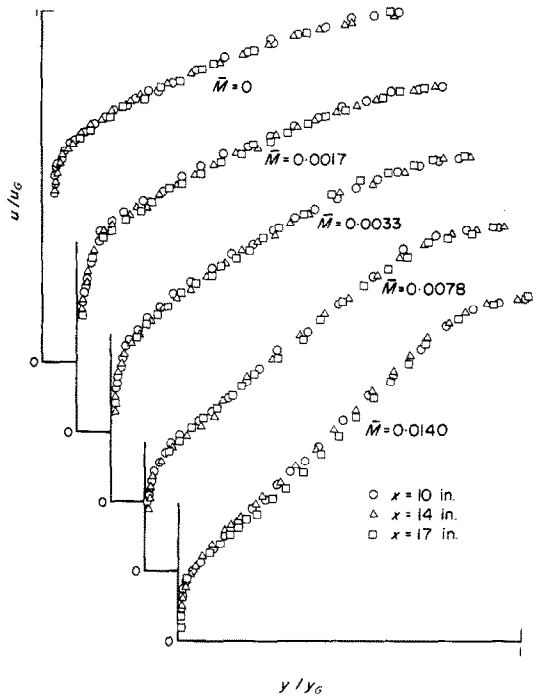

FIG. 16. Freon injection velocity profiles.

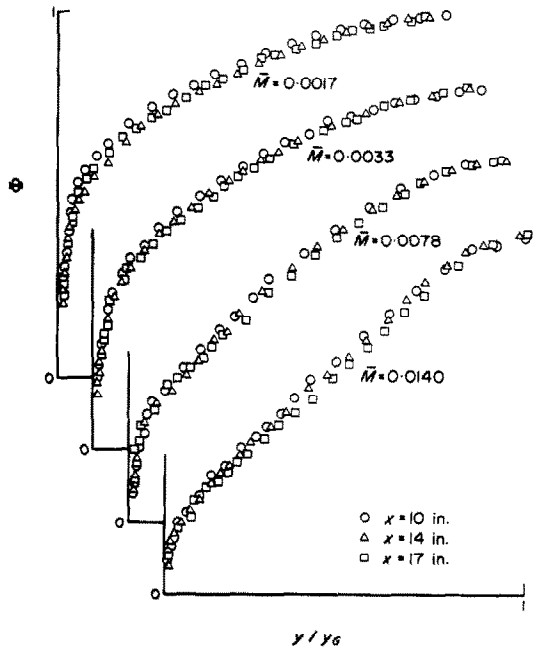

FIG. 17. Freon injection concentration profiles.

would not conform with the data shown in Fig. 19; for as M tends to zero the profile must approach that appropriate to an impermeable wall.

Profiles of mixing length distribution, obtained in the same way as for air injection, are shown in Fig. 20. Evidently the very steep gradients in density near the wall have no influence on the variation of mixing length: a linear variation with slope of 0·425 fits the data very well. Over the outer region too, the trend of the data is much the same as for air injection showing a decrease in l with increase in M and with distance downstream (with the sole exception of the profile for $M = 0{\cdot}0078$). Figure 21 shows the value

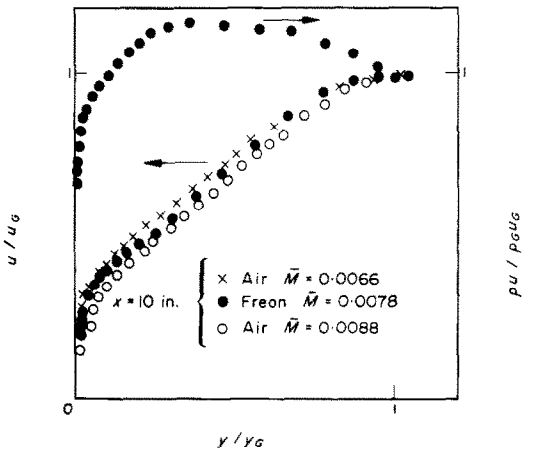

FIG. 18. Comparison of freon and air velocity profiles.

of l half-way across the boundary layer plotted as a function of R_{max}, a Reynolds number based upon Y_G and $\sqrt{(\tau_{max}/\rho)}$ which are arguably the appropriate length and velocity scales for the outer region of the layer. The figure shows that there is a systematic decrease of (l/Y_G) with Reynolds number for R_{max} less than 10^3. At higher Reynolds numbers the mixing length appears to level off. The same trends are shown for both the air and freon injection though at the higher injection rates the freon data show slightly lower values of l. The formula

$$l = 0{\cdot}075 y_G(1 + \exp[-0{\cdot}0025\, R_{max}])$$

fits both the freon and air data quite well considering the inherent imprecisions in obtaining mixing-length distributions from processing mean velocity (and density) profiles. This formula is employed in [6] as one element in a model of turbulence used for extensive predictions of transpired flows.

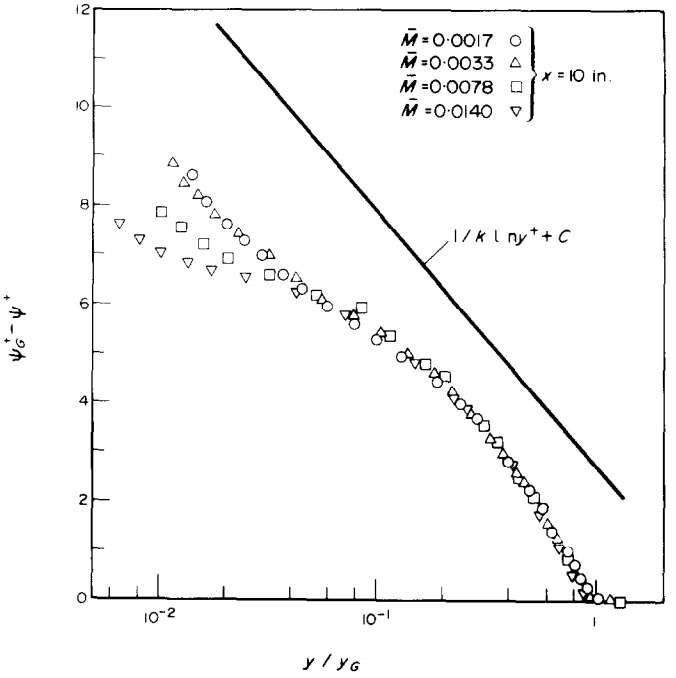

FIG. 19. Freon injection velocity-defect profiles.

Figure 22 brings out an interesting difference between the effects of air and freon injection on the skin friction coefficient and Stanton number. It is evident that nearly twice the level of freon injection is required to reduce the friction coefficient by the same amount as for air injection. The Stanton number curve is, however, virtually unaffected by the density ratio. Finally, Fig. 23 shows the distribution of the turbulent Prandtl/Schmidt number across the boundary layer for four freon injection rates and at three stations. The general trend of the data shows a smooth decrease from the wall to the outer edge of the boundary layer in close agreement with the variation proposed by Rotta; there is no consistent dependence of σ_t on injection rate. About 80 per cent of the data fall within the uncertainty envelope suggested by Simpson *et al.* [18] obtained from heat transfer measurements for air injection, with the centre of gravity of our data about 7 per cent higher than those of [18] over the inner half of the layer and virtually coincident with it over the outer half. The density ratio across the boundary layer reaches 4·0:1 for the highest freon injection rates. It is therefore rather encouraging (from the point of view of providing a simple model of transpired boundary layers) that the turbulent Schmidt number and mixing length distributions should turn out to be effectively the same as in a uniform density boundary layer on an impermeable wall.

SUMMARISING REMARKS

The following are the main findings to have emerged from this study:

(a) Over the range of experiments where the present work and that of Simpson *et al.* [3] overlap, close agreement is observed between the investigations, specifically regarding:

(i) the influence of M on the level of friction coefficient,

(ii) the dependence of the additive function in the $\psi^+ \sim y^+$ relationship on v_w^+.

(iii) the universality of the outer region in transpired-velocity-defect coordinates

(iv) the distribution of turbulent Schmidt number across the boundary layer.

(b) Numerical reprocessing of Simpson's data however has confirmed Squire's [4] finding that the quoted values of c_f are not consistent with the measured variation of momentum thickness.

(c) The slow withdrawal of fluid through the porous surface (withdrawal velocity less than 0·25 per cent

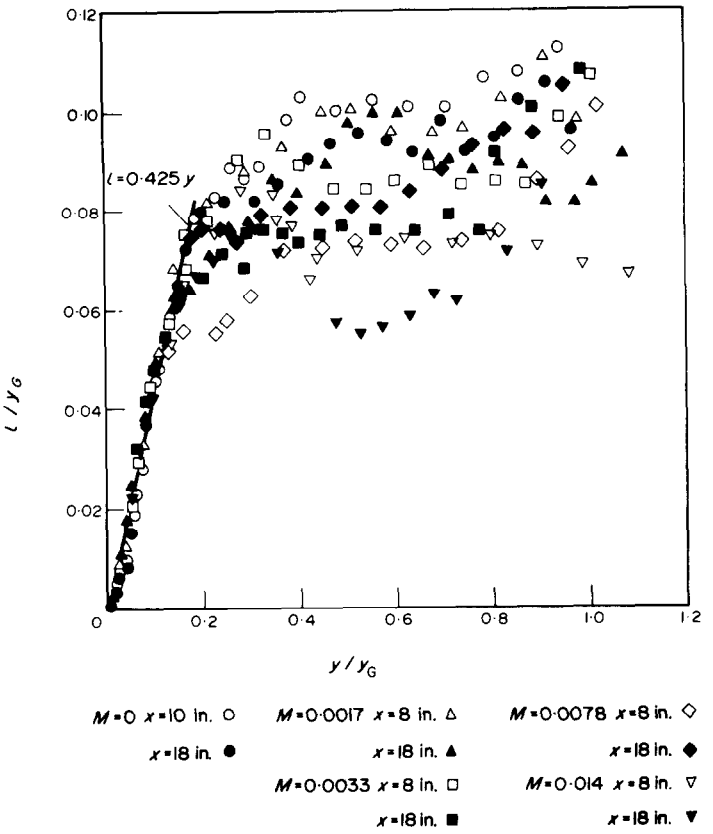

FIG. 20. Mixing length distributions for various freon injection rates in zero pressure gradient.

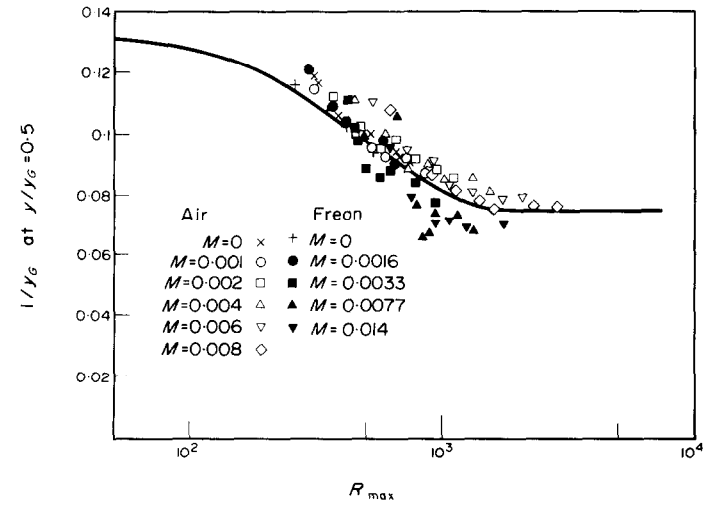

FIG. 21. Mixing length ratio as a function of the turbulent Reynolds number R_{max}.

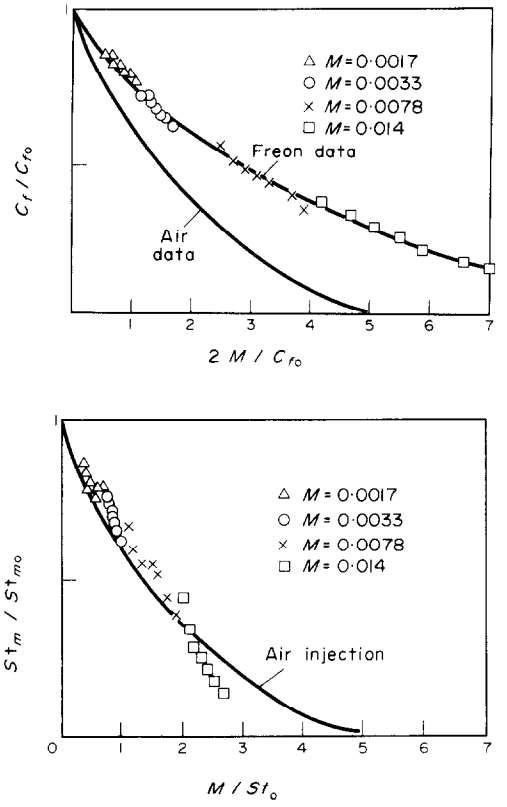

FIG. 22. Skin friction and Stanton number variations for freon injection.

of free stream velocity) provided a satisfactory method of measuring the value of wall concentration.

(d) With freon injection the velocity and concentration profiles are self-preserving for a given level of M. Velocity profiles are not discernibly different from those for air injection at the same level of blowing.

(e) With moderate or hign rates of freon injection, the outer region of the boundary layer is again sensibly independent of the level of blowing when velocity profiles are compared in transpired velocity defect coordinates.

(f) About twice the level of blowing is needed with freon to cause the same reduction in c_f as for air.

(g) The mixing length distribution across the boundary layer is not directly dependent on injection rate or transverse density gradients. The indirect influence of these parameters is attributable to their effect on the turbulence Reynolds number in the outer part of the flow.

Acknowledgements—The research has been fully supported by the Procurement Executive, Ministry of Defence; we express our thanks to the Ministry for the interest and support given to the work and for permission to publish the findings. The initial portion of the research programme, including the design of the test section was supervised by Dr. V. K. Jonsson whose contribution we gratefully acknowledge.

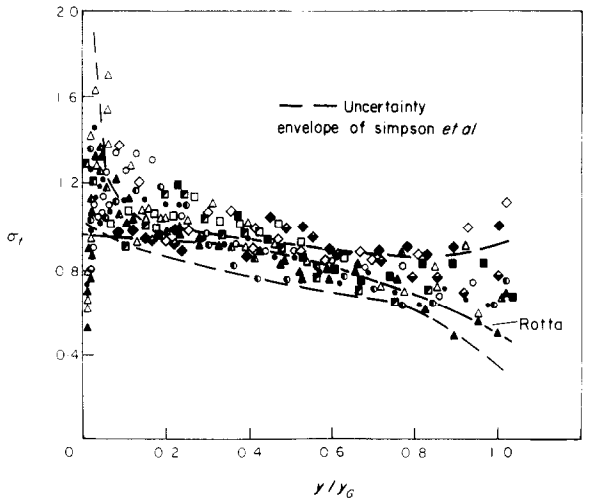

$M = 0{\cdot}0017$	$x = 6$	$M = 0{\cdot}0078$	$x = 6$
	$x = 10$		$x = 10$
	$x = 14$		$x = 14$
$M = 0{\cdot}0033$	$x = 6$	$M = 0{\cdot}014$	$x = 6$
	$x = 10$		$x = 10$
	$x = 14$		$x = 14$

FIG. 23. Turbulent Prandtl/Schmidt number distributions for freon injection in zero pressure gradient.

REFERENCES

1. M. S. Mickley and R. S. Davis, Momentum transfer over a flat plate with blowing NACA TN 4017 (November 1957).
2. V. K. Jonsson and C. J. Scott, Uniform air injection into a turbulent boundary layer flow over an axial circular cylinder, University of Minnesota HTL-TR-63 (July 1965).
3. R. L. Simpson, W. M. Kays and R. J. Moffat, The turbulent boundary layer on a porous plate: an experimental study of the fluid dynamics with injection and suction, University of Stanford Rept. No. HMT-2 (December 1967).
4. L. C. Squire, The constant property turbulent boundary layer with injection; a reanalysis of some experimental results, *Int. J. Heat Mass Transfer* **13**, 939 (1970).
5. D. Dunbar and L. C. Squire, Correlations of concentrations, temperature and velocity profiles in compressible turbulent boundary layers, with foreign gas injection.
6. R. J. Baker and B. E. Launder, The turbulent boundary layer with foreign gas injection: II Predictions and measurements in severe streamwise pressure gradients, *Int. J. Heat Mass Transfer* **17**, 293 (1974).
7. T. N. Stevenson, Inner region of transpired turbulent boundary layers, *AIAA Jl* **6**(3) (1967).
8. J. McQuaid, Experiments on incompressible turbulent boundary layers with distributed injection, ARC 28735 (January 1967).
9. T. J. Black and A. J. Sarnecki, The turbulent boundary layer with suction or injection, ARC 20, 501 (October 1958).
10. M. W. Rubesin, An analytical estimation of the effect of transpiration cooling on the heat transfer and skin-friction characteristics of a compressible turbulent boundary layer NACA TN 3341 (December, 1954).
11. E. R. Van Driest, On mass transfer near the stagnation point, AFOSR Rep. TN-57-458 (1967).
12. V. C. Patel, Calibration of the Preston tube and limitations on its use in pressure gradients, *J. Fluid Mech.* **23**, pt 1, (1965).
13. D. B. Spalding and S. W. Chi, The drag of a compressible turbulent boundary layer on a smooth flat plate with and without heat transfer, *J. Fluid Mech.* **18**, pt. 1 (1964).
14. D. E. Coles, The turbulent boundary layer in a compressible fluid, RAND Rept. R-403-PR (September 1962).
15. M. P. Escudier, The distribution of mixing length in turbulent flow near walls, Imperial College, Mech. Eng. Dept. Rep. TWF/TN/1 (1966).
16. R. J. Baker, The turbulent boundary layer with streamwise pressure gradient and foreign gas injection, Ph.D Thesis, University of London (1971).
17. R. J. Moffat and W. M. Kays, The turbulent boundary layer on a porous plate: experimental heat transfer with uniform blowing and suction. Stanford University Rept. No. HMT-1 (August 1967).
18. R. L. Simpson, D. G. Whitten and R. J. Moffat, An experimental study of the turbulent Prandtl number of air with injection and suction, *Int. J. Heat Mass Transfer* **13**, 125 (1970).
19. D. E. Tewfik, Some characteristics of the turbulent boundary layer with air injection, *AIAA Jl* (6) (1963).
20. V. K. Jonsson and C. J. Scott, Uniform air injection into a turbulent boundary layer flow over an axial circular cylinder, University of Minnesota HTL-TR-63 (July 1965).
21. C. C. Pappas and A. F. Okuno, The relation between skin friction and heat transfer for the compressible turbulent boundary layer with gas injection, NASA TN D-2857 (June 1965).
22. M. W. Rubesin, An analytical estimation of the effect of transpiration cooling on the heat transfer and skin-friction characteristics of a compressible turbulent boundary layer, NACA TN 3341 (December 1954).
23. K. Torii, N. Nishiwaki and M. Hirata, Heat transfer and skin friction in turbulent boundary layers with mass injection, Proceeding third Int. Heat Transfer Conference, Vol. 3 and 6 (August 1966).
24. M. S. Mickley and R. S. Davis, Momentum transfer for flow over a flat plate with blowing, NACA TN 4017 (November 1957).
25. R. M. Kendall, M. W. Rubesin, T. J. Dahm and M. R. Mendenhall, Mass momentum and heat transfer within a turbulent boundary layer with foreign gas mass transfer at the surface, Part 1—constant fluid properties, VIDYA AD 619 209 (February 1964).
26. W. H. Dorrance and F. J. Dore, The effect of mass transfer on the compressible turbulent boundary-layer skin friction and heat transfer, *J. Aero. Sci.* **21**, (1954).
27. S. S. Kutateladze and A. I. Leont'ev, *Turbulent Boundary Layers in Compressible Gases.* Arnold.

APPENDIX I

Shear Stress and Flux D stribution

The shear stress distribution $\tau(y)$ is determined by partially integrating the boundary layer equation to a point in the layer, as follows:

$$\tau = \tau_w + \int_0^y \left(\rho u \frac{\partial u}{\partial x} + \rho v \frac{\partial u}{\partial y} + \frac{\mathrm{d}p}{\mathrm{d}x}\right) \mathrm{d}y \qquad \text{(A.1)}$$

which, upon elimination of $\mathrm{d}p/\mathrm{d}x$ with the Bernoulli equation, may be manipulated to:

$$\tau = \tau_w + \int_0^y \left[\frac{\partial \rho u^2}{\partial x} + \rho_w v_w u - u \frac{\partial}{\partial x}\left(\int_0^y \rho u \mathrm{d}y\right) - \frac{1}{u}\frac{\partial u}{\partial x}\right] \mathrm{d}y \qquad \text{(A.2)}$$

if

$$\frac{1}{u}\frac{\partial u}{\partial x}$$

is approximated by

$$\frac{1}{U_G}\frac{\mathrm{d}U_G}{\mathrm{d}x}$$

then the shear stress distribution may be derived as follows:

$$\frac{\tau_w - \tau}{\rho_G U_G^2} = \frac{\mathrm{d}\delta_{2y}}{\mathrm{d}x} - \frac{Mu}{U_G} + \frac{1}{U_G}\frac{\mathrm{d}U_G}{\mathrm{d}x}\left(\frac{U}{U_G}\delta_{1y} + \delta_{2y}\right) \qquad \text{(A.3)}$$

where δ_{1y} and δ_{2y} are the displacement and momentum thicknesses associated with the region $0 \rightarrow y$ in the boundary

	$M \times 10^3$	$C_f \times 10^3$ (at $R_x = 10^6$)	x_0(in)	aR_x^b	$\left(\frac{\text{Standard deviation}}{\delta_2}\right)\%$ (3rd Order poly)	No. profiles
Present data	0	1·85	3·0	0·20	0·54	8
	1·0	1·35	2·8	0·19	0·34	7
	2·1	1·05	2·2	0·20	0·45	7
	4·4	0·52	1·3	0·06	0·10	7
Simpson*	0	1·91	7·8	0·65	1·48	8
		(1·89)	(0)	(2.3)		
	1·0	1·57	6·9	0·51	1·02	7
		(1·54)	(0)	(2.5)		
	1·9	1·15	3·8	0·73	0·77	8
		(1.20)	(0)	(1.7)		
	3·8	0·65	1·7	0·68	1·89†	4†

* Original values in parenthesis [3].
† 2nd order polynomial.

layer. With the last term on the right of (A.3) written as P_y, the equation simplifies to:

$$\frac{c_{fy}}{2} = \frac{c_f}{2} - \frac{d\delta_{2y}}{dx} + \frac{MU_y}{U_G} + P_y \tag{A.4}$$

where

$$\frac{c_{fy}}{2} = \tau/\rho_G U_G^2.$$

In this form the equation reduces to the standard momentum integral equation as $y \to y_G$. Finally, following [3] we further assume that*

$$\frac{1}{\delta_{2y}}\frac{d\delta_{2y}}{dx} = \frac{1}{\delta_2}\frac{d\delta_2}{dx}. \tag{A.5}$$

The shear stress distribution then simplifies to a form involving only cross-stream integrals:

$$\frac{\tau}{\tau_w} = \left(1 - \frac{\delta_{2y}}{\delta_2}\right) + \frac{2M}{c_f}\left(\frac{u}{U_G} - \frac{\delta_{2y}}{\delta_2}\right) + \frac{2P}{c_f}\left(\frac{P_y}{P} + \frac{\delta_{2y}}{\delta_2}\right) \tag{A.6}$$

where P denotes the value of P_y at $y = y_G$.

The flux distribution may be derived in a similar manner to give:

$$\frac{J}{J_w} = \left(1 - \frac{\delta_{2my}}{\delta_{2m}}\right) + \frac{M}{St_m}\left(\Phi - \frac{\delta_{2my}}{\delta_{2m}}\right) + \frac{p_m}{St_m}\left(\frac{p_{my}}{p_m} + \frac{\delta_{2my}}{\delta_{2m}}\right) \tag{A.7}$$

where subscript m refers to the mass species equation, and P_{my} denotes:

$$\frac{\delta_{2my}}{u_G}\frac{du_G}{dx}.$$

* Sample calculations indicated the approximation was valid well within 5 per cent.

APPENDIX 2

Skin Friction Determination

As y tends to y_G equation (A.4) reduces to the momentum integral equation, as follows:

$$\frac{c_f}{2} = \frac{d\delta_2}{dx} - P - M. \tag{A.8}$$

The main difficulty in using this equation to determine c_f from experimental data lies in the numerical differentiation of δ_2 in the streamwise direction. For a zero pressure gradient turbulent boundary layer on an impermeable flat plate $d\delta_2/dx$ can probably be determined to within ∓ 4 per cent (see for example the plot c_f in Fig. 5). For adverse pressure gradients and injection, where both P and M are positive, the magnitude of $d\delta_2/dx$ and P and M are all of the same order, and errors in c_f can become very large. In these circumstances the basic form assumed for the $\delta_2(x)$ variation has marked effect on the results of a least squares analysis of the experimental data. Most workers assume a polynomial variation of δ_2 with x, although at least a 3rd-order polynomial (requiring at least 7 profile measurements) is the minimum requirement for a satisfactory fit of the data, and even then polynomials only give a 'good' fit in the middle of the data.

References [16] and [3] concluded that over a small range of R_x a power law relation of the following form was more appropriate:

$$R_{\delta 2} = aR^b_{x+x_0}. \tag{A.9}$$

This implies that for a relatively constant injection rate the $c_f - R_x$ distribution is linear on log–log co-ordinates. A detailed discussion of the method is given in [16]. Here it may suffice to remark that to employ this method we need a value of x_0, the distance from the porous section at which the boundary may be supposed to originate. Simpson *et al.* [3] assumed that the virtual origin for all transpiration rates was coincident with the start of the transpired region. For high injection rates this assumption is adequate, but for most of his (and certainly our own) tests, x_0 is not negligible.

The present method consisted of iterating on the three parameters a, b and x_0 to obtain the minimum standard deviation of the data. For the case where transpiration and pressure gradient were both zero the value of b turned out to be very close to 0·8, a commonly accepted value.

The following table shows some typical c_f results obtained at $R_x \approx 10^6$ at various injection rates. The results are compared with the original data of Simpson [3] at similar injection rates, and also recalculated values of Simpson's data using the present procedure. The standard deviation of the data using equation (A.9) is also compared with that obtained from a 3rd order polynomial.

DIE TURBULENTE GRENZSCHICHT MIT GAS-AUSBLASUNG I. MESSUNGEN OHNE DRUCKGRADIENT

Zusammenfassung—Es wird über die Ergebnisse einer experimentellen Untersuchung der turbulenten Grenzschicht mit Massenzufuhr durch die Wand berichtet. Es wurden zwei Injektions-Gase verwendet, nämlich Luft und Freon, mit Massenströmen bis zu 0,8% des Freistrahlstromes.

Für Luft-Ausblasung sind die vorliegenden Daten in sehr guter Übereinstimmung mit Messungen von Simpson u.a. [3]. Es ergibt sich ein schwächerer Einfluss der Ausblasung auf die Wandreibung als auf die anderen Grössen der Strömung.

Für die Freon-Ausblasung sind die gemessenen Geschwindigkeitsprofile nur wenig verschieden von denen, die man erhält, wenn die gleiche Luftmenge ausgeblasen wird, obwohl die Dichteunterschiede zwischen Wand und Freistrahl bei Freon-Ausblasung bis 4:1 gehen. Geschwindigkeits- und Konzentrationsprofile werden nach kurzer Anlaufstrecke stabil. Ein Vergleich der Verteilung der Mischungsweglänge und der turbulenten Schmidt-Zahl zeigt ebenfalls keine deutlichen Unterschiede gegenüber den Strömungen mit konstanter Dichte.

COUCHE LIMITE TURBULENTE AVEC INJECTION DE GAZ ÉTRANGER—I. MESURE AVEC GRADIENT DE PRESSION NULLE

Résumé—On présente les résultats expérimentaux d'une étude sur le développement d'une couche limite avec injection pariétale de masse. On réalise l'injection d'air et de fréon avec une vitesse égale à 0,8 pour cent de la vitesse massique de l'écoulement au loin.

Dans le cas de l'injection d'air les résultats sont en étroit accord avec ceux de Simpson et Coll [3] montrant un effet plus important de l'injection sur le coefficient de frottement local que dans les autres recherches sur cet écoulement.

En ce qui concerne l'injection de fréon, bien que la variation de densité entre la paroi et l'écoulement au loin est dans le rapport 4:1, les profils de vitesse sont peu différents de ceux obtenus avec la même vitesse d'air injecté. Les profils de vitesse et de concentration sont tous deux affinés après une région initiale de développement. Les distributions de longueur de mélange et de nombre de Schmidt turbulent ne montrent pas de différence sensible avec celles qui correspondent aux écoulements à densité uniforme.

ТУРБУЛЕНТНЫЙ ПОГРАНИЧНЫЙ СЛОЙ ПРИ ВДУВЕ ИНОРОДНОГО ГАЗА 1. ИЗМЕРЕНИЯ ПРИ НУЛЕВОМ ГРАДИЕНТЕ ДАВЛЕНИЯ

Аннотация—В статье представлены результаты экспериментального исследования развития турбулентного пограничного слоя с поверхностным вдувом воздуха и фреона; приведенная скорость вдува составляла до 0,8% скорости свободного потока.

Полученные данные по вдуву воздуха очень хорошо согласуются с измерениями Симпсона и др [3], в исследованиях которого показано более слабое влияние вдува на локальный коэффициент поверхностного трения по сравнению с другими аналогичными работами.

При вдуве фреона, когда плотность внешнего потока и плотность газа в пристеночной области имеют соотношение 4:1, измеренные профили скоростей мало отличаются от профилей, полученных при вдуве воздуха, подаваемого с той же интенсивностью. Профили средней скорости и профили концентрации становятся развитыми за зоной короткого начального участка. Сравнение распределений длины смешения турбулентных чисел Шмидта также указывает на отсутствие заметного различия от рапределений, полученных в потоках равномерной плотности.